JOURNAL OF GEOPHYSICAL RESEARCH, VOL. 103, NO. B2, PAGES 2585–2596, FEBRUARY 10, 1998

Cellular convection models of mid-ocean ridge hydrothermal circulation and the temperatures of black smoker fluids

William S. D. Wilcock

School of Oceanography, University of Washington, Seattle

Abstract. Mid-ocean ridge hydrothermal vent fields are characterized by maximum sustained venting temperatures of 320°-380°C, irrespective of the spreading rate and the inferred depth of circulation. Metamorphic assemblages, fluid inclusions, oxygen isotope data, and the salinity of vent fluids have all been used to infer maximum circulation temperatures of up to 500°-700°C. In this paper I investigate the pattern of circulation and the relationship between venting and basal temperatures using simple models of steady open-top porous convection in a rectangular medium heated from below. Solutions obtained with variable fluid properties which approximate seawater include much more recirculation than solutions obtained with uniform fluid properties, and the temperatures of upwelling fluids are greater. For a uniform permeability, models obtained with seawater properties yield a ratio of the venting temperature to the bottom temperature in the range 0.5-0.65, values which are reasonably consistent with the observations. However, a surficial layer of high permeability significantly reduces vent temperatures. Since extrusive basalts are almost certainly very permeable, this result seems incompatible with the existence of black smoker vents. It has been suggested previously that the precipitation of hydrothermal minerals where hot and cold fluids meet will lead to the formation of an impermeable shell around upflow zones. Such a shell may provide a means to tap hot fluids from depth.

1. Introduction

It is well established that hydrothermal circulation is the primary mechanism responsible for cooling young oceanic crust. Black smoker hot springs are the most spectacular manifestation of this process and have been observed at ~20 locations on the global mid-ocean ridge system [*Fornari and Embley*, 1995; *Humphris*, 1995; *Von Damm*, 1995]. Along fast spreading ridges such as the East Pacific Rise (EPR), high-temperature vents are confined to a narrow zone enclosing the axial summit caldera [*Haymon et al.*, 1991]. Seismic data reveals the presence of a small magma chamber located at 1-2 km depth beneath the ridge axis [*Detrick et al.*, 1987, 1993], a feature which appears to be steady state on some segments [*Scheirer and Macdonald*, 1993]. Although the geometry of hydrothermal circulation is incompletely known, petrological observations from mid-ocean ridges [*Alt*, 1995] and ophiolites [*Richardson et al.*, 1987; *Nehlig and Juteau*, 1988] suggest that the region of most intense high-temperature alteration occurs near the dike-gabbro transition just above the axial magma chamber. Along slow spreading ridges such as the Mid-Atlantic Ridge, active vent fields can be located well away from the neovolcanic zone [*Rona et al.*, 1986], magma chambers are transitory features [*Sinton and Detrick*, 1992; *Solomon and Toomey*, 1992], and high-temperature venting is not clearly tied to shallow magma bodies. The presence of earthquakes at depths up to 8 km beneath the axial valley [*Toomey et al.*, 1985; *Kong et al.*, 1992; *Wolfe et al.*, 1995] suggests that hydrothermal fluids circulate near the Moho. However, despite the apparent difference between the depth of axial hydrothermal circulation on slow and fast spreading ridges, maximum venting temperatures are remarkably similar. Transitory temperatures above 400°C have been observed following an eruption at 9°50'N on the EPR [*Von Damm et al.*, 1995] and for very short periods elsewhere [e.g., *Delaney et al.*, 1984], but maximum sustained temperatures fall in the range 320°-380°C [*Von Damm*, 1995] (Figure 1).

If it is assumed that hydrothermal fluids rise quickly and follow adiabatic paths, the observed range of venting temperatures extrapolates to 325°-400°C at the depth of the EPR magma chambers and 340°-440°C at the Moho (Figure 1). Mineral solubility experiments and theoretical phase relations [*Berndt et al.*, 1989; *Seyfried et al.*, 1991] suggest that reaction zone temperatures of 375°-410°C at pressures of 40 MPa (i.e., 4 km below sealevel) are required to reproduce the chemistry of hot spring fluids. Thus it appears that all but the hottest vent fluids cool conductively while ascending to the seafloor [*Berndt et al.*, 1989; *Seyfried et al.*, 1991]. However, these thermodynamic temperatures reflect the last equilibrium between hydrothermal fluid and altered oceanic crust and are not necessarily the maximum temperature of hydrothermal circulation. There is good evidence that the temperatures at the base of hydrothermal systems reach higher values. In some fields, large deviations of salinity from seawater may be best explained by two-phase separation at supercritical pressures [*Delaney et al.*, 1987; *Cowan and Cann*, 1988; *Von Damm*, 1988; *Bischoff and Rosenbauer*, 1989]. Evidence from metamorphic assemblages [*Gillis and Robinson*, 1990; *Stakes et al.*, 1991; *Gillis and Thompson*, 1993; *Gillis et al.*, 1993; *Nehlig*, 1994; *Manning et al.*, 1996], fluid inclusions [*Kelley and Robinson*, 1990; *Nehlig*, 1991; *Kelley et al.*, 1993; *Saccocia and Gillis*, 1995], and oxygen isotope data [*Gregory and Taylor*, 1981; *Stakes and Vanko*, 1986; *Stakes*, 1991; *Stakes and Taylor*, 1992], obtained from both mid-ocean ridges and ophiolites, suggests that hydrothermal fluids circulate to maxi-

Paper number 97JB03252.
0148-0227/98/97JB-03252$09.00

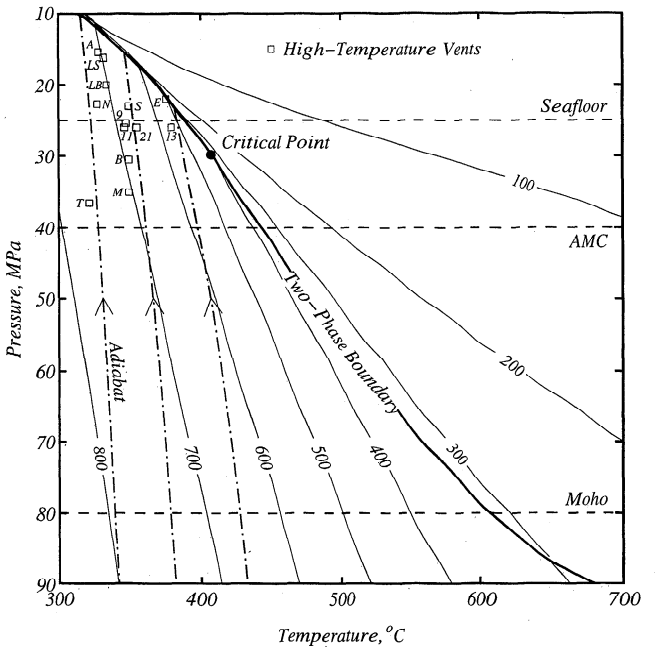

Figure 1. Phase diagram for seawater (3.2 wt % NaCl solution) [*Pitzer et al.*, 1984; *Anderko and Pitzer*, 1993] showing the location of the two-phase boundary (bold solid line), the critical point (solid circle), and density contours (kg m^{-3}). In the two-phase region the density is that of the two-phase mixture. The pressures and maximum sustained temperatures of black smoker fields on unsedimented ridges are shown as labeled open squares where the labels refer to vent fields as follows: 9, East Pacific Rise (EPR) 9°50'N; 11, EPR 11°N; 13, EPR 13°N; 21, EPR 21°N; S, South Cleft; N, North Cleft; A, Axial Volcano; E, Endeavour; M, MARK (Snakepit); T, TAG; B, Broken Spur; LS, Lucky Strike; and LB, Lau Basin. All the temperature data is from *Von Damm* [1995] except for the Endeavour [*Butterfield et al.*, 1994] and the EPR near 9°50'N [*Von Damm et al.*, 1995]. Dashed horizontal lines show the approximate hydrostatic pressures for the seafloor at 2400 m depth, an upper crustal magma chamber (AMC), and the Moho. Near-vertical dot-dashed lines show adiabats for venting temperatures of 320°, 350°, and 380°C [*Pitzer et al.*, 1984; *Anderko and Pitzer*, 1993].

mum temperatures of at least 500°C at mid-crustal depths and up to 700°C in the lower crust.

One explanation for both the uniformity of maximum venting temperatures and for differences between the maximum temperatures of venting and circulation is that hydrothermal circulation forms a two-layer double-diffusive system [*McNabb and Fenner*, 1985; *Bischoff and Rosenbauer*, 1989]. *Bischoff and Rosenbauer* [1989] argue that supercritical phase separation results in the formation of a dense layer of convecting brine at temperatures of 450-700°C, overlain by a single-pass seawater cell. Highly saline fluid inclusions with formation temperatures of up to 700°C are, in fact, observed in gabbros from mid-ocean ridges [*Stakes and Vanko*, 1986; *Kelley and Delaney*, 1987] and ophiolites [*Nehlig*, 1991; *Kelley et al.*, 1992]. However, these inclusions do not prove the existence of a large brine layer because the fluids may be magmatic [*Kelley and Delaney*, 1987; *Kelley et al.*, 1992]. Numerical models suggest that double-diffusive systems may be unstable in low-porosity media [*Rosenberg*, 1991] and that phase-separated brines may be flushed out before large volumes accumulate. Simple physical models of the brine layer suggest that it may have a lifetime of years to centuries [*Lowell and Germanovich*, 1997]. Time series observations following volcanic eruptions [*Butterfield and Massoth*, 1994; *Von Damm et al.*, 1995; *Butterfield et al.*, 1997] demonstrate that the residence times of brines formed by diking events are fairly short.

If the stable pattern of convection is single-layer circulation, then an alternative explanation must be found for the uniformity of maximum venting temperatures. *Lister* [1974, 1983] argues that the maximum temperature of circulation is determined by the rigidus, the temperature at which rocks crack because ductile creep rates are insufficient to accommodate thermal contraction. Because the lithology of oceanic crust is relatively uniform, the rigidus must be relatively constant although its value is not well known [*Hayba and Ingebritsen*, 1997]. On the basis of observations of fluid pressures in boreholes at several sites including Nesjavelier, Iceland, *Fournier* [1991] argues for value of 370-400°C, while *Lister* [1974, 1983] suggests ~500°C. If the physical characteristics of porous convection result in venting temperatures that are a fixed fraction of the bottom temperature, which is itself fixed, then the temperatures of black smokers might be explained quite simply.

Numerous models of cellular convection beneath mid-ocean ridges have been published for both uniform fluid properties [*Ribando et al.*, 1976; *Rosenberg and Spera*, 1990; *Rosenberg et al.*, 1993] and pure water [*Fehn and Cathles*, 1979; *Fehn et al.*, 1983; *Brikowski and Norton*, 1989; *Travis et al.*, 1991], but none of these studies have addressed venting temperatures in detail. In this paper I present solutions for steady cellular convection in two-dimensional open-top models with pressure- and temperature-dependent fluid properties which approximate seawater. The models are single phase but are extended into the two-phase region by choosing properties which approximate the two-phase mixture. The results are used to investigate the relationship between venting and basal temperatures.

2. The Model

Figure 2 shows the configuration of the two-dimensional models considered in this paper. Convection is confined to a porous rectangular region of height H and width γH and is driven by a vertical temperature difference ΔT. The bottom boundary is isothermal and impermeable; the top boundary is permeable and isobaric; and the side boundaries are periodic so that fluids exiting from one side reenter on the other. I investigate two models with different types of thermal conditions on the top boundary. In the first model the top boundary is isothermal. This is the appropriate boundary condition for a Darcy continuum overlain by a constant temperature ocean but has the disadvantage that fluids which exit the model are always cold. In the second model, hot fluids are allowed to vent at the seafloor by replacing the isothermal top boundary condition in the region of upflow with a vertical temperature gradient of zero (i.e., no heat exits the top of the upflow zone by conduction) [*Forster and Smith*, 1988].

The equations which describe one-phase Darcy flow through a porous medium are the conservation of mass, momentum, and energy

$$\frac{\partial \rho_f}{\partial t} + \nabla.(\rho_f \mathbf{u}) = 0 \tag{1}$$

$$\mathbf{u} = -\frac{k}{\mu}(\nabla p + \rho_f g \hat{\mathbf{z}}) \tag{2}$$

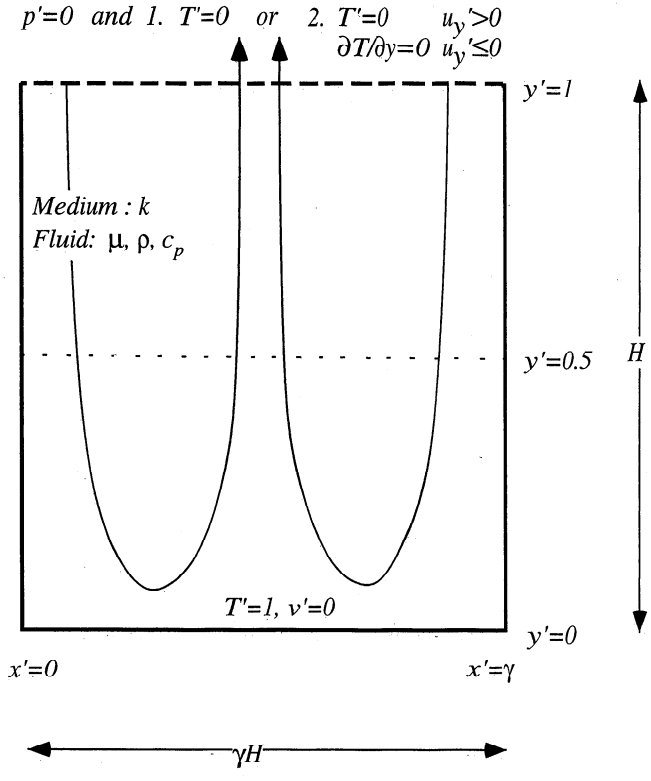

Figure 2. Configuration of the numerical models.

$$\rho_m c_{p,m}\frac{\partial T}{\partial t}+\rho_f c_{p,f}(\mathbf{u}.\nabla T)=\lambda_m\nabla^2 T \tag{3}$$

where the notation here and throughout this section is defined in the notation section. Because hydrothermal fluids in the upwelling (and downwelling) plumes generally fall in the one-phase region where the adiabatic gradients are fairly small (Figure 1), the adiabatic term has been excluded from (3).

Equations (1)-(3) can be solved most simply if the thermodynamic and transport properties are taken to be constant except for the fluid density which is represented by the Boussinesq approximation. In this approach the density is assumed constant everywhere except in the buoyancy term of (2) where it is approximated by a linear function of temperature

$$\rho_f=\rho_0[1-\alpha_f(T-T_0)] \tag{4}$$

The conservation equations can be nondimensionalized by substituting the following nondimensional variables denoted by primes

$$\mathbf{x}=H\mathbf{x}'$$
$$T=T_0+\Delta T T'$$
$$t=\frac{H^2}{\kappa}t'$$
$$\mathbf{u}=\frac{\kappa}{H}\mathbf{u}' \tag{5}$$
$$p=\frac{\kappa\mu}{k}p'$$

where the thermal diffusivity κ is defined

$$\kappa=\frac{\lambda_m}{\rho_f c_{p,f}} \tag{6}$$

After subtracting from (2) the hydrostatic pressures that result from a conductive vertical temperature gradient, (1)-(3) reduce to

$$\nabla.\mathbf{u}'=0 \tag{7}$$

$$\mathbf{u}'=-\nabla' p'+RaT'\hat{\mathbf{z}} \tag{8}$$

$$\sigma\frac{\partial T'}{\partial t'}+\mathbf{u}.\nabla T'=\nabla'^2 T' \tag{9}$$

where Ra is the Rayleigh number

$$Ra=\frac{k\rho_0\alpha\Delta T g H}{\mu\kappa} \tag{10}$$

and σ is the ratio of volumetric heat capacity for the saturated porous medium to that of the fluid

$$\sigma=\frac{\rho_m c_{p,m}}{\rho_f c_{p,f}} \tag{11}$$

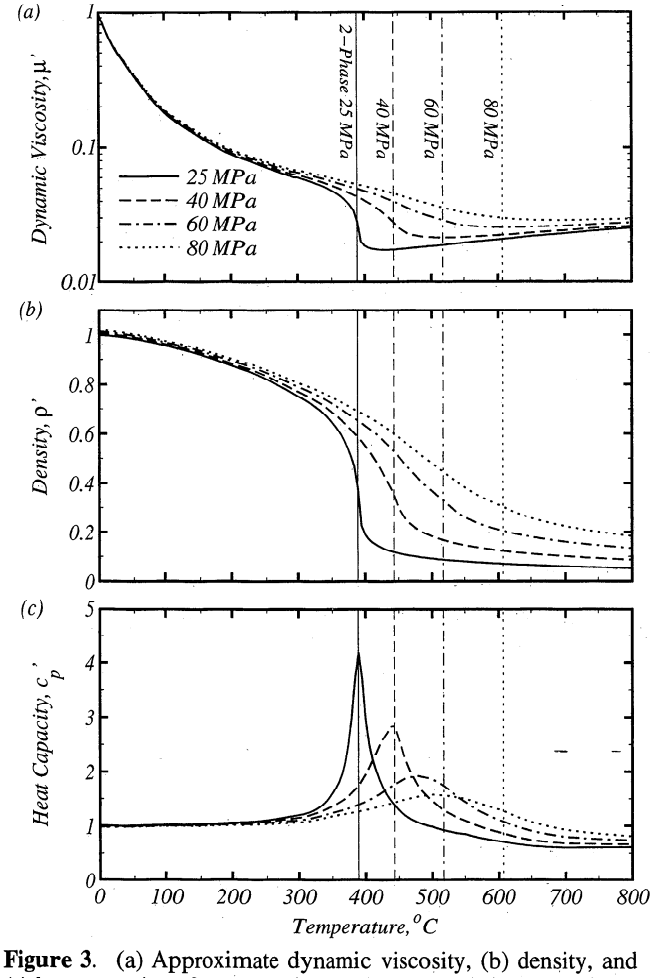

Figure 3. (a) Approximate dynamic viscosity, (b) density, and (c) heat capacity of seawater in nondimensional units as a function of temperature at 25 (solid), 40 (dashed), 60 (dot-dashed), and 80 MPa (dotted). Vertical lines show the temperatures of the two-phase boundary. The dynamic viscosity is calculated using an expression for pure water [*Meyer et al.*, 1993], while the density and heat capacity are those for a 3.2 wt % NaCl solution [*Pitzer et al.*, 1984; *Anderko and Pitzer*, 1993]. Properties have been normalized to reference values at 0°C and 250 MPa.

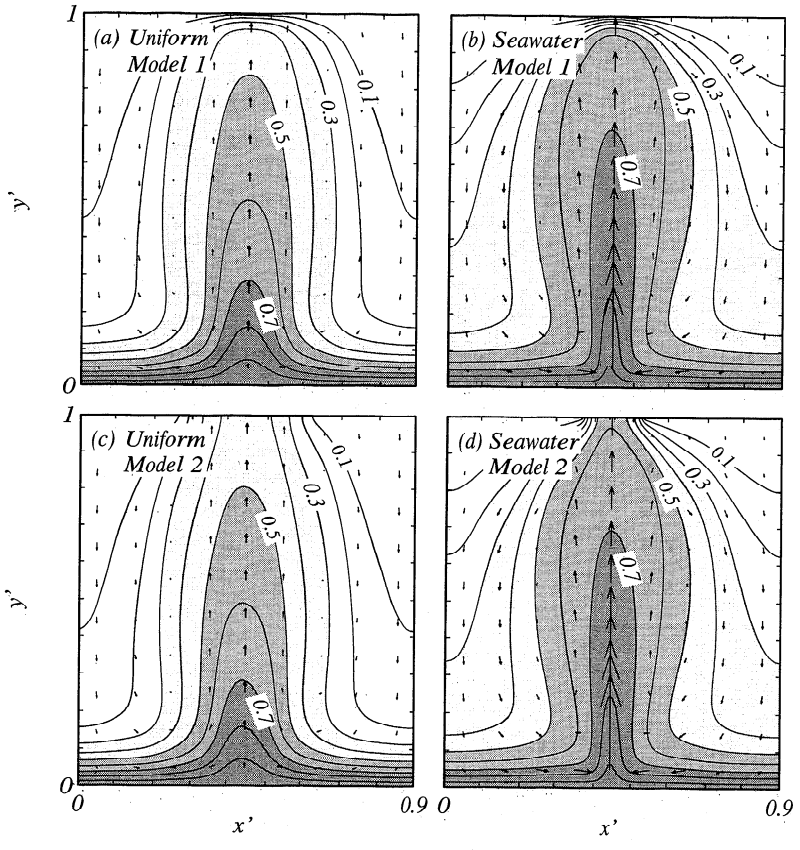

Figure 4. Solutions for steady cellular convection at an aspect ratio of 0.9 and a Nusselt number of 6. Contours and shading show the nondimensional temperature structure and arrows show the relative magnitude and direction of flow and are scaled uniformly on all plots. (a) The fluid properties are uniform and the top boundary has a fixed temperature. (b) The same as for Figure 4a except the properties approximate seawater for top and bottom pressures of 25 and 40 MPa, respectively, and a bottom temperature of 500°C. (c-d) The same as for Figures 4a and 4b, respectively, except the second type of top thermal boundary condition is used.

The density, dynamic viscosity, and specific heat capacity of seawater (Figure 3) are not well represented by a fluid with uniform properties. The viscosity decreases by an order of magnitude between 0 and 200°C and continues to decrease until temperatures enter the two-phase region; the density decreases very nonlinearly with temperature; and the heat capacity is strongly peaked, reaching a maximum near the two-phase boundary. Because seawater densities at high temperatures are only a small fraction of cold seawater, the assumptions underlying the Boussinesq approximation are not satisfied. Nonuniform fluid properties can be incorporated into the nondimensional formulation by including the following variables

$$c_p(T,p) = c_{p0}c_p'(T',p')$$
$$\mu(T,p) = \mu_0\mu'(T',p') \qquad (12)$$
$$\rho(T,p) = \rho_0\rho'(T',p')$$

Substitution of equations (5) and (12) into equations (1)-(3) yields

$$\frac{\partial \rho_f'}{\partial t'} + \nabla'\cdot(\rho_f'\mathbf{u}') = 0 \qquad (13)$$

$$\mu'\mathbf{u}' = -\nabla' p' + \frac{k\rho_0 g H}{\mu_0\kappa_0}\rho''\hat{\mathbf{z}} \qquad (14)$$

$$\sigma_0\rho_m'c_{p,m}'\frac{\partial T'}{\partial t'} + \rho_f'c_{p,f}'(\mathbf{u}'\cdot\nabla' T') = \nabla'^2 T' \qquad (15)$$

A Rayleigh number can still be defined for this formulation using (10) provided μ, α, and κ are defined at standard conditions but its numerical value is dependent on where the standard fluid properties are defined [*Sorey*, 1978]. It is more useful to characterize solutions by the Nusselt number which is the ratio of the observed vertical heat transport to that which would occur by conduction alone.

In this study I solved (13)-(15) numerically using a finite-volume formulation with a relaxation solver [*Patankar*, 1980]. The algorithm has been benchmarked against analytical solutions and published numerical results [*Cherkaoui et al.*, 1997]. Because accurate solutions for unsteady patterns of flow require considerable computational resources, I considered only steady flow by excluding the first term from (13) and (15). For models of the second type the top thermal boundary condition was updated each iteration as the solver converged to the steady state solution. Thus the position of the upflow zone was not fixed a priori. At Nusselt numbers exceeding 8, the numerical solutions did not converge well, an indication that the true pattern of flow is unsteady. This study was limited to Nusselt numbers below this threshold. The solutions presented in this paper were all obtained with a mesh of 96 x 96 control volumes. The cell spacing is uniform in the horizontal direction, while in the vertical direc-

tion the cell spacing decreases near the top and bottom boundaries in order to better resolve the boundary layers. Grid refinement experiments with uniform and nonuniform meshes of up to 192 x 192 cells were used to check that the solutions were adequately resolved spatially.

The thermodynamic properties of seawater were approximated using a 3.2 wt % NaCl solution [*Bischoff and Rosenbauer*, 1985] and the equations of state of *Anderko and Pitzer* [1993] and *Pitzer et al.* [1984] above and below 300°C, respectively. Within the two-phase region the thermodynamic properties were those of the mixture. The viscosity was calculated using a formula for pure water [*Meyer et al.*, 1993] in which the independent variables are temperature and density. Within the two-phase region the density assumed for the viscosity calculation was that of the volumetrically dominant phase. Measurements of the viscosity of sodium chloride solutions at high temperatures and pressures [*Yusufova et al.*, 1978] show that the viscosity of seawater differs only slightly from pure water. The fluid properties were incorporated into the numerical algorithm by means of linear interpolation between the values in a lookup table with temperature and pressure intervals of 10°C and 0.5 MPa, respectively.

3. Results

3.1. Effects of Seawater Fluid Properties

Figure 4 shows cellular convection solutions for both models with uniform and seawater fluid properties. Each plot shows the pattern of steady convection in a box of aspect ratio 0.9 at a Nusselt number of 6. The seawater properties are for top and bottom pressures of 25 and 40 MPa, respectively, and a bottom temperature of 500°C. Except for the region near the surface of the upwelling plume the choice of the top thermal boundary conditions has little effect on the pattern of convection. For both types of model the use of seawater properties significantly increases temperatures in the upwelling plume. At middepth ($y' = 0.5$) the maximum nondimensional temperature increases from 0.60 to 0.73. The reasons for this increase can be understood by considering the processes that occur at the base of the cell and in the upwelling plume. The bottom thermal boundary layer is a region of steep temperature gradients and fluid moves through this region horizontally before being swept upward. Horizontal conduction acts to cool the core of the upwelling plume, and the maximum temperature at its center is dependent on its velocity and width and the relative proportions of fluid which enter the plume at different temperatures. When seawater properties are included, the hottest fluids near the bottom of the boundary layer are very buoyant and have a low viscosity. As a result the proportion of the hottest fluids entering the plume increases since they rise more quickly. The high heat capacity of fluids near the two-phase boundary also acts to buffer the temperature as the upwelling plume cools.

It is also apparent from the flow vectors in Figure 4 that the variable viscosity of seawater significantly influences the pattern of circulation. For uniform viscosity the flow in the upwelling and downwelling plumes is nearly vertical, and there is very little fluid exchange between the plumes. For variable viscosity, there is significant horizontal flow near the surface, which results in recirculation and broadens the high-temperature region. Qualitatively, this change in the flow pattern occurs because the viscosity of seawater decreases quickly at moderate temperatures (Figure 3). Although the warm fluids at the edge of the upwelling

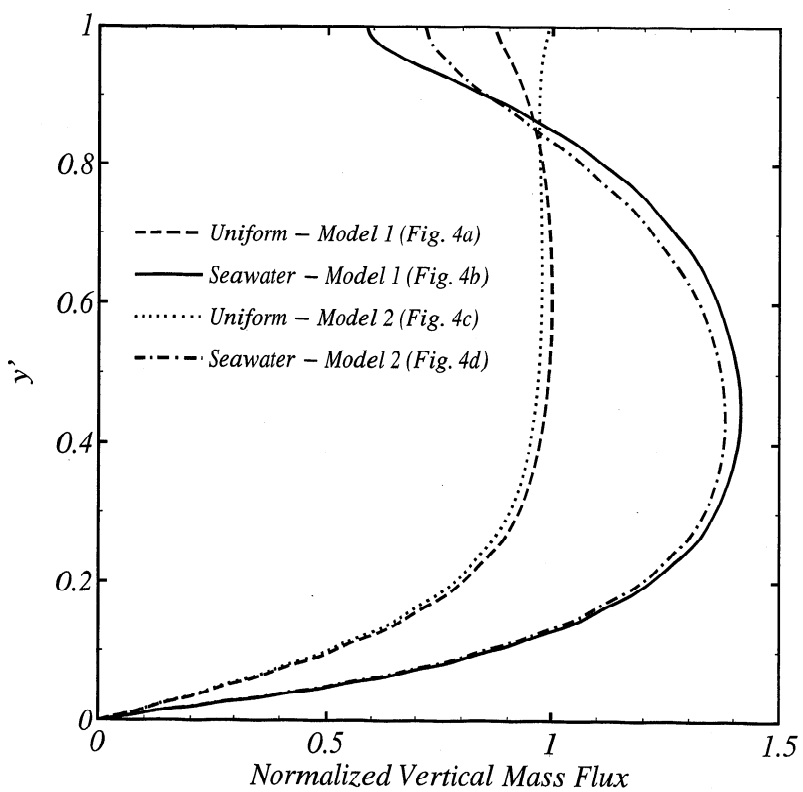

Figure 5. Normalized mass fluxes passing upward (or downward) across a horizontal plane as a function of height for the solutions shown in Figure 4. The fluxes have been normalized to the maximum value in the solution of Figure 4a.

plume are relatively buoyant when compared to the cold fluids that enter through the top boundary, there is less resistance to recirculating warm fluids because they have a substantially lower viscosity. Recirculation can be quantified by considering the mass flux of fluid that moves upward (or downward) across a horizontal plane as a function of depth within the model (Figure 5). Except near the surface the choice of the top boundary condition has only a small effect on the mass fluxes. For uniform fluid properties the surface fluxes are very similar to those at middepths, while for seawater properties about half the fluid moving up across the horizontal plane $y' = 0.4$ recirculates.

While studying Rayleigh-Bernard convection, *Malkus* [1954] hypothesized that when several solutions to the convection equations are possible, the preferred pattern of flow will maximize the heat transport. Although this hypothesis may not be strictly correct for turbulent convection at very high Rayleigh numbers [*Malkus*, 1996], theoretical and experimental work suggests that it holds for steady state patterns of flow at moderate Rayleigh numbers [*Malkus and Veronis*, 1958; *Schlüter et al.*, 1965]. In the numerical solutions presented here the width of the cells is determined by the dimensions of the model. The Malkus hypothesis implies that if solutions were obtained for an infinite horizontal layer, the observed spacing of plumes would maximize the Nusselt number. Figure 6 shows the Nusselt number as a function of aspect ratio for seawater fluid properties and Rayleigh numbers which were chosen to give maximum Nusselt numbers near 4, 6, and 8. At higher Nusselt numbers, solutions for steady flow do not converge completely because the true pattern of flow is unsteady. The preferred aspect ratio decreases with increasing Rayleigh number.

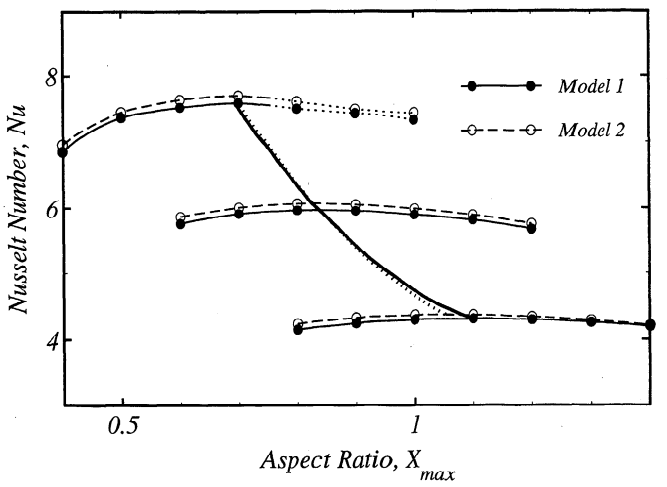

Figure 6. Nusselt number as a function of cell aspect ratio (width divided by height) for seawater properties with top and bottom pressures of 25 and 40 MPa, respectively, and a bottom temperature of 500°C. Curves are plotted for both types of top thermal boundary conditions and Rayleigh numbers (defined at 25 MPa and 0°C) of 19, 37, and 58, which were chosen because they yield maximum Nusselt numbers near 4, 6, and 8. Note that for higher aspect rations the solutions with Nusselt numbers near 8 did not converge well and are connected by a dotted line. Bold curves connect the aspect ratios which maximize the Nusselt number. *Malkus* [1954] hypothesizes that the aspect ratio that maximizes heat transport will be preferred when convection occurs in an infinite horizontal medium.

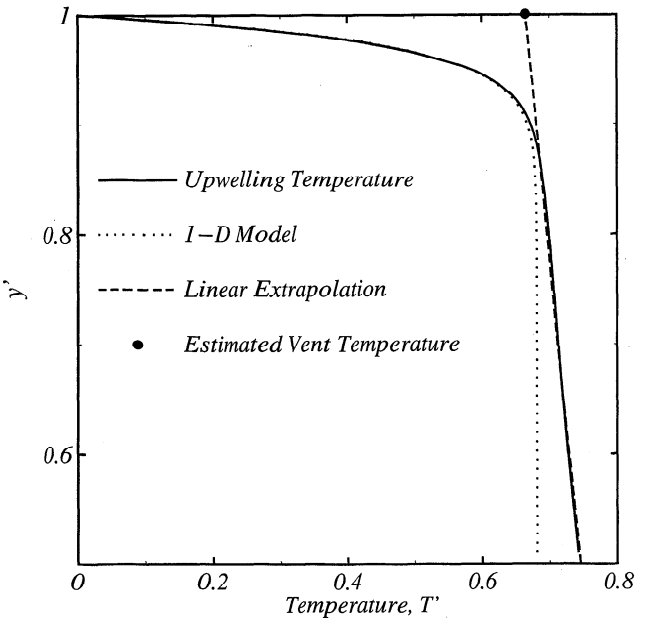

Figure 7. Example showing the method used to estimate maximum vent temperatures from cellular convection solutions with a fixed temperature top boundary condition. The solid curve shows the nondimensional temperature as a function of height in the center of the upwelling plume of Figure 4b. The cold boundary condition at the top of the model results in the formation of a thin thermal boundary layer in which temperatures increase quickly with depth. Here the temperature structure is reasonably well approximated by the simple one-dimensional model (dotted curve). If the fluids initially at a nondimensional temperature T'_{deep} upwell at a uniform Darcy velocity V' toward an isothermal permeable boundary at $y' = 1$ and $T' = 0$, the temperature is given by $T(y') = T'_{deep} \exp[1-(y'-1)/V']$ [e.g., *Schlichting*, 1979]. The curve was obtained by setting V' equal to the maximum velocity in the thermal boundary layer and by adjusting T'_{deep} to optimize the fit. Beneath the boundary layer the temperature in the models is not constant as the one-dimensional model predicts but increases approximately linearly with depth because horizontal conduction cools the fluids. A maximum venting temperature (solid circle) can be estimated from the cellular convection solutions by a linear extrapolation to the surface (dashed curve).

3.2. Venting Temperatures

The fixed temperature boundary condition at the top of the first model requires that venting fluids be cold and is obviously inconsistent with seafloor observations. Inspection of the solutions (Figures 4a and 4b) shows that a thermal boundary layer forms at the top of the upwelling plume. The top boundary condition used in the second model eliminates this inconsistency but also implies incorrectly that the seafloor is hot throughout the upflow zone. Both models fail because the continuum hypothesis underlying the equations for Darcy convection break down near the surface. Along mid-ocean ridges, high-temperature fluids exit at high velocities from well-spaced orifices and are no longer in thermal equilibrium with all the surrounding rock. In some sense the two models bracket the true thermal conditions near the top of the upflow zone because in reality the average temperatures will fall between the two models. I therefore chose to estimate maximum venting temperatures for both types of model. For the second model these come directly from the solution. For

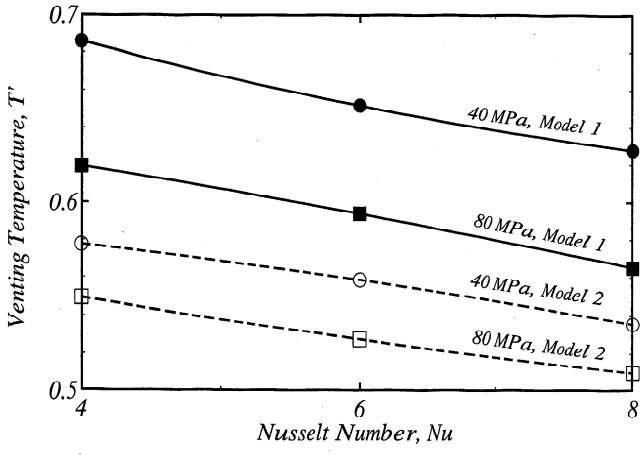

Figure 8. Maximum nondimensional venting temperature as a function of Nusselt number for both models and bottom pressures of 40 and 80 MPa. The top pressure is 25 MPa, and the bottom temperature is 500°C.

the first I assume that black smokers tap fluids which are unaffected by surface cooling and estimate a venting temperature by extrapolating from beneath the surficial surface boundary layer (Figure 7).

At a given Nusselt number the dimensionless venting temperatures are fairly insensitive to the aspect ratio. Figure 8 shows the venting temperature as a function of Nusselt number for an aspect ratio of 0.9 for both models and for two different bottom pressures. Venting temperatures estimated for models with a fixed temperature top boundary condition are higher than those for the second model. It can be seen from Figure 4 that the top thermal boundary condition results in enhanced near-surface cooling by horizontal conduction. For both models the venting temperature decreases with Nusselt number. Figure 9 shows the variations in nondimensional venting temperatures as a function of bottom temperature at a Nusselt number of 6. For bottom temperatures of 600°C and below, the nondimensional venting temperatures ranges from 0.52 to 0.65. The maximum nondimensional venting temperatures are observed for a bottom temperature of 500-600°C. At higher temperatures the venting temperature decreases quite sharply.

It is well established that the permeability of oceanic crust varies with depth [*Anderson et al.*, 1985]. Solutions for two-layered permeability models with uniform fluid properties have been presented before [*Rosenberg and Spera*, 1990; *Rosenberg et al.*, 1993] but were not specifically used to estimate venting temperatures. Figure 10 shows two solutions obtained with seawater properties and a two-layer model in which the permeability of the top layer k_t is either 100 (Figure 10a) or 0.1 (Figure 10b) times the permeability of the bottom layer k_b. The patterns of convection differ markedly from those obtained with a uniform permeability (Figure 4). In each solution the Darcy velocities are relatively large in the high-permeability layer, while the temperature gradients are larger in the low-permeability layer. As a consequence the model with a high-permeability top layer is characterized by a low venting temperature and vice versa. Figure 11 shows nondimensional venting temperatures as a function of the permeability ratio of the top to bottom layers. As the permeability ratio increases from 0.01 to 1000, the venting temperature decreases from ~0.7 to 0.1.

4. Discussion

In this paper I have presented solutions for porous convection in an open-top rectangular box using fluid properties that approximate seawater. The results have been used to investigate the relationship between venting temperatures and bottom temperatures. It is clear that these simple solutions for two-dimensional Darcy convection grossly simplify the processes which control the physical characteristics of circulation in real systems. Before comparing the models to observed temperatures of black smoker fluids I summarize the limitations of the models.

4.1. Model Limitations

The equations for Darcy flow on which the models are based depend on the assumption that the permeability can be represented by a continuum. Because fluid fluxes tend to be dominated by flow through the widest cracks, cellular convection solutions will approximate real flow patterns only when the scale under consideration greatly exceeds the fracture spacing. As I noted above, the continuum assumption clearly breaks down near the surface in the upflow zone where flow is focused into black smoker conduits. Here the details of flow can be modeled on small scales by including high-permeability conduits [*Yang et al.*, 1996], if the geometry is known. On a larger scale the critical length (if any) at which the continuum assumption holds has not been determined for mid-ocean ridge systems.

Even if the large-scale permeability structure can be represented by a continuum, the assumption of a uniform or two-layered permeability is an oversimplification. Not only does the permeability of oceanic crust decrease progressively with depth over the upper 2 km [*Anderson et al.*, 1985], but fault zones are likely to produce significant lateral variations as well. Evidence from ophiolites [*Nehlig and Juteau*, 1988], seafloor observations [*Haymon et al.*, 1991], and the shapes of vent fields [*Wilcock and McNabb*, 1995] suggest that the crust is strongly anisotropic. Two-dimensional numerical solutions show that anisotropy can significantly influence the patterns of flow [*Rosenberg and Spera*, 1990; *Rosenberg et al.*, 1993]. In real systems the permeability will be influenced by chemical reactions [*Richardson et*

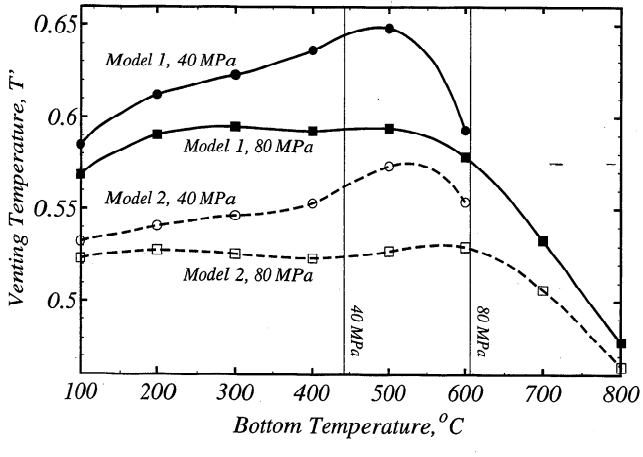

Figure 9. Maximum nondimensional venting temperatures as a function of bottom temperature for both types of model and bottom pressures of 40 and 80 MPa. The top pressure is 25 MPa, and the bottom temperature is 500°C.

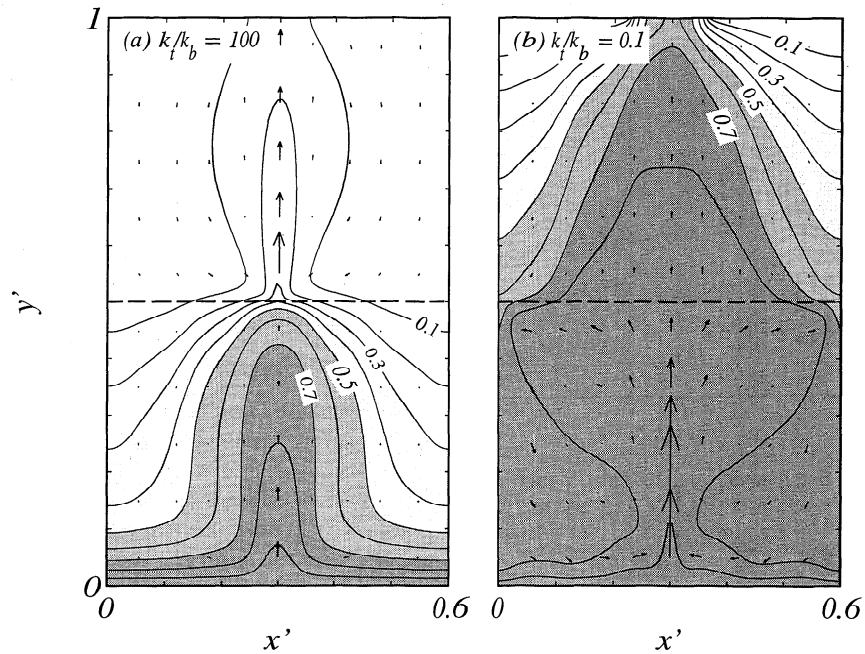

Figure 10. Solutions for steady cellular convection at an aspect ratio of 0.6 and a Nusselt number of 6 for two-layer permeability models in which the layers have equal thickness. Both solutions have the second type of top thermal boundary condition. The fluid properties approximate those of seawater at top and bottom pressures of 25 and 40 MPa, respectively, and a bottom temperature of circulation of 500°C. (a) The ratio of the permeability in the top layer to the bottom layer is 100 and (b) the ratio is 0.1. The roughness apparent in the temperature contours near the base of the second solution is a result of poor model converge which indicates the true pattern of flow may include an unsteady component. Labeled contours and shading show the nondimensional temperature structure, and arrows show the relative magnitude and direction of flow and are scaled uniformly on both plots.

al., 1987; *Richards et al.*, 1989] and tectonism, processes that may preclude steady state circulation over long periods. Previous work shows that silica [*Wells and Ghiorso*, 1991; *Lowell et al.*, 1993] and anhydrite [*Sleep*, 1991] precipitation can have significant effects on the pattern of flow.

The validity of Darcy's law is also dependent on the existence of laminar flow, an assumption that is favored by thin cracks. Black smoker vents are fed by wide conduits in which the flow is clearly turbulent. However, because crack spacings and widths probably decrease with depth [*Goldfarb and Delaney*, 1988; *Nehlig*, 1994] and the cold downwelling fluids have a relatively high viscosity (Figure 3), turbulent flow may be confined to the shallower portions of upflow zones.

The single-phase solutions presented here incorporate fluid properties which approximate seawater. In the two-phase region the models are based on thermodynamic properties which match those of the two-phase mixture and a viscosity which approximates that of the volumetrically dominant phase. While the brine phase which would form at the base of the models is a minor component volumetrically, it is unknown whether it has a significant effect on characteristics of large-scale flow. A single-phase model cannot address the long-term fate of the brine.

The models include a fixed temperature on the lower boundary. This is a reasonable boundary condition if the maximum temperature of circulation is controlled by a fixed rigidus temperature below which rocks crack [*Lister*, 1974, 1983]. However, at high Nusselt numbers the heat flux can only be maintained if the lower boundary migrates downwards at a velocity equal to about one fifth of the mean Darcy flow velocity [*Lister*, 1974, 1983]. If hydrothermal circulation does not deepen with time, a fixed flux boundary condition may be more appropriate [*Lowell and Germanovich*, 1994].

Steady state models are limited to maximum Nusselt numbers of 8 since at higher values the solutions do not converge because the pattern of flow is unsteady. A Nusselt number of 8 is compatible with steady state models of fast spreading ridges [*Phipps Morgan and Chen*, 1993] and is certainly sufficient to match fluxes of ~1-10 MW estimated for isolated black smokers [*Little et al.*, 1987]. However, the Nusselt numbers for circulation beneath large black smoker fields are almost certainly higher. Heat flux estimates of ~100-1000 MW for the Main Endeavour vent field suggests circulation with a Nusselt number of at least 100 [*Wilcock and Delaney*, 1996]. This study shows that nondimensional venting temperatures decrease as the Nusselt number increases (Figure 8). Whether this trend continues when the flow enters the unsteady regime is unknown.

4.2. Venting Temperatures

Despite the uncertainties that must arise from the simplifying assumptions underlying the model the results do illustrate some interesting relationships between vent temperatures and bottom temperatures. Because hydrothermal fluids rise quickly and the appropriate adiabatic gradients are small, it is sometimes assumed that temperatures measured in black smokers can be equated to those in the reaction zone [e.g., *Bischoff and Rosenbauer*, 1989]. However, for all the models presented in this study the predicted venting temperatures are significantly lower than bottom temperatures for two reasons. First, only the fluids which circulate right to the bottom of the system reach the bot-

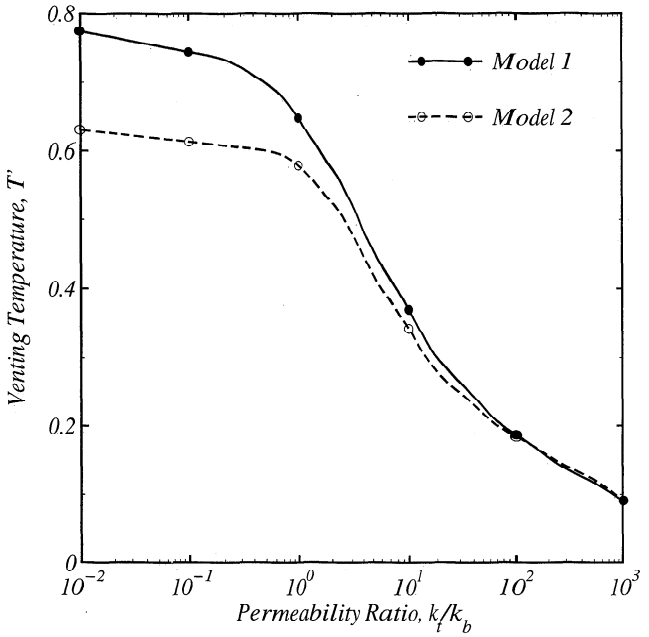

Figure 11. Maximum nondimensional venting temperatures as a function of the permeability ratio in the two-layer model for solutions with an aspect ratio of 0.6 and a Nusselt number of 6. Results are shown for both types of top thermal boundary conditions, top and bottom pressures of 25 and 40 MPa, respectively, and a bottom temperature of 500°C.

tom temperature. The average temperature of fluids entering the upflow zone is significantly lower (Figure 4). Second, the fluids in the upflow zone cool by lateral conduction. This result is in good agreement with chemical evidence that vent fluids have cooled by tens of degrees [*Berndt et al.*, 1989; *Seyfried et al.*, 1991]. For models with uniform permeability and bottom temperatures up to 700°C the maximum venting temperature is equal to 0.5-0.65 of the bottom temperature (Figure 9). Applying this result to mid-ocean ridges, the observed maximum venting temperatures of 320-380°C (Figure 1) require bottom temperatures of 490°-760°C, in reasonable agreement with inferred maximum temperatures of circulation of 500°-700°C.

This interpretation is too simplistic because the venting temperatures are very sensitive to the vertical permeability structure. For a two-layer model, nondimensional venting temperatures decrease from 0.7 to 0.1 as the ratio of the permeability in the top to bottom layers increases from 0.01 to 1000 (Figure 11). In continental systems the reaction zone is commonly a region of high permeability overlain by a relatively impermeable layer [*White*, 1973]. This configuration (Figure 10b) results in an isothermal reaction zone and high vent temperatures. Along mid-ocean ridges such a permeability distribution could account for the uniformity of maximum venting temperatures if the reaction zones feeding black smokers were near 500°C.

However, in situ observations for oceanic crust off axis show that permeabilities decrease with depth by several orders of magnitude in the upper 2 km [*Anderson et al.*, 1985]. On-bottom gravity [*Luyendyk*, 1984; *Holmes and Johnson*, 1993] and seismic [*Christeson et al.*, 1994] measurements have been used to infer layer 2A porosities of ~20% on axis, values which imply extremely high permeabilities. In the numerical models, upwelling fluids entering a surficial layer of high permeability, cool rapidly and the resulting vent temperatures are low (Figures 10a and 11). This result is consistent with the results of earlier numerical models [*Rosenberg*, 1991; *Rosenberg et al.*, 1993] and with the inference of several workers that diffuse low-temperature venting dominates the axial hydrothermal heat flux [*Rona and Trivett*, 1992; *Schultz et al.*, 1992; *Baker*, 1994; *Schultz et al.*, 1996] but seems incompatible with both the chemistry of low-temperature fluids and the presence of black smokers.

In the models the fluids which vent at low temperatures follow relatively shallow paths and never reach high temperatures. In contrast the chemistries of low-temperature fluids sampled at Galapagos [*Edmond et al.*, 1979] and TAG [*James and Elderfield*, 1996] require that they are mixtures of a high-temperature endmember and seawater. However, it is certainly possible that low temperature fluids with the characteristics predicted by the numerical models do exist. Because seafloor sampling strategies generally focus on high-temperature vents, relatively few low-temperature fluids have been sampled. Furthermore, low-temperature diffuse venting is generally detected by observing the associated biology. The vent biota is supported primarily by hydrogen sulfide [e.g., *Tunnicliffe*, 1992] and it has not been determined if, and under what circumstances, this chemical will be present in seawater which circulates to maximum temperatures of a few tens of degrees Celsius. Studies of metamorphic assemblages from DSDP Hole 504B [*Alt et al.*, 1986a, b] and the Troodos ophiolite [*Gillis and Robinson*, 1988, 1990] provide extensive evidence for circulation at high water/rock ratios in the volcanic section at temperatures of 0-150°C. Indeed, schematic models of flow paths inferred from such studies (e.g., Figure 14 in *Alt* [1995]) are very similar to Figure 10a.

The equations for Darcy flow do not include mixing which occurs in real systems because of the tortuous and intersecting nature of the flow paths. This effect which is referred to as thermal dispersion [*Nield and Bejan*, 1992], can be modeled by an enhanced conductivity. Thus conduction and mixing have similar physical effects. The preponderance of mixed low-temperature fluids near high-temperature vents demonstrates that cooling by thermal dispersion is more important in these regions than conductive cooling. However, including thermal dispersion in the numerical models would not result in a better estimate of maximum vent temperatures because the hottest fluids generally have chemistries which require no mixing with seawater and thus no cooling by thermal dispersion [*Von Damm*, 1995].

On the basis of observations of stockworks in the Troodos ophiolite [*Richardson et al.*, 1987], *Cann and Strens* [1989] argue that mineral precipitation in subsurface regions where hot fluids cool leads to the formation of a clogged shell enclosing the discharge zone. When fully formed, such a shell inhibits mixing by sealing high-temperature upflow from downflow and may provide a means to tap high-temperature fluids to the surface through a generally high permeability layer. The model of *Cann and Strens* [1989] clearly simplifies the complex nature of the alteration processes that occur in stockworks [*Richardson et al.*, 1987; *Richards et al.*, 1989]. However, the fact that high-temperature fluids show no sign of mixing lends support to the concept that the high-temperature fluids can follow isolated paths.

Water column studies on the Mid-Atlantic Ridge between 36° and 38°N [*German et al.*, 1996] detected 7 sites of hydrothermal venting, 5 of which are located in highly tectonized locations near segment boundaries. *German et al.* [1996] note that many earlier studies failed to search for vents near segment boundaries and argue that the sites of high-temperature fields are controlled by tectonism and often coincide with the intersecting fabrics as-

sociated with ridge discontinuities. Tectonism clearly does play an important role in controlling the local sites of venting [*Delaney et al.*, 1992; *Kleinrock and Humphris*, 1996], but models of magmatic segmentation would predict higher heat fluxes near the segment centers [e.g., *Batiza*, 1996]. I suggest that the unexpected prevalence of hydrothermal venting near segment ends is consistent with a larger fraction of the local hydrothermal heat flux being liberated as high-temperature fluids at these locations. Here the volcanic layers are fairly thin (or absent) [e.g., *Batiza*, 1996], and thus the cooling effects of a high-permeability upper layer may be diminished. In contrast, the extrusive layers are thick near segment centers, and high-temperature fluids may only reach the seafloor if circulation is sufficiently long-lived to build up extensive stockworks.

5. Conclusions

I have presented a numerical model of one-phase hydrothermal circulation beneath mid-ocean ridges. As for any simple model of a complex system, the solutions have limitations, but they do lead to a number of conclusions.

1. Estimated maximum venting temperatures obtained with fluid properties which approximate seawater are up to 50% higher than those obtained with uniform fluid properties, and the flow pattern includes much more recirculation.

2. In all solutions presented, vent temperatures are significantly lower than bottom boundary temperatures. The difference between maximum vent temperatures of 320°-380°C and maximum inferred reaction zone temperatures of 500°-700°C is not, in and of itself, conclusive evidence for two-layer double-diffusive circulation.

3. In the numerical model a high-permeability surface layer leads to low vent temperatures. *Cann and Strens* [1989] argue that impermeable shells will form around high-temperature upflow zones because of the precipitation of quartz and sulfide minerals in regions where the hot fluids cool. Because layer 2A probably has a very high permeability, an impermeable shell which isolates upwelling fluids may well be a prerequisite for high-temperature venting.

4. Future models should investigate unsteady flow at higher Nusselt numbers, two-phase flow, three-dimensional anisotropy, the effects of chemical reactions on permeability, and turbulent upflow. Because each effect adds significant numerical complexity, they are probably best studied separately.

Notation

Symbols

c_p	Specific heat capacity.
g	Acceleration of gravity.
H	Layer thickness.
k	Permeability.
p	Pressure.
t	Time.
T	Temperature.
$\boldsymbol{u}$	Darcy velocity.
$\hat{\mathbf{z}}$	Unit vector pointing upward.
α	Volumetric coefficient of thermal expansion.
γ	Model aspect ratio (width divided by height).
ΔT	Temperature difference across layer.
κ	Thermal diffusivity.
λ	Thermal conductivity.
μ	Dynamic viscosity.
ρ	Density.

Subscripts

b	Properties of the bottom layer in a two-layer model.
f	Properties of the fluid.
m	Properties of the saturated porous media.
t	Properties of the top layer in a two-layer model.
0	Properties at reference temperature, T_0.

Acknowledgments. I thank A. Fisher, S. Ingebritsen, and M. Tivey for very thorough reviews and J. Baross, A. Cherkaoui, J. Delaney, D. Kelley, M. Lilley, R. McDuff, and J.-C. Sempéré for useful discussions. This work was supported in part by NSF grant OCE-9529425.

References

Alt, J. C., Subseafloor processes in mid-ocean ridge hydrothermal systems, in *Seafloor Hydrothermal Systems: Physical, Chemical, Biological, and Geological Interactions, Geophys. Monogr. Ser.*, vol. 91, edited by S. E. Humphris et al., pp. 85-114, AGU, Washington, D. C., 1995.

Alt, J. C., J. Honnorez, C. Laverne, and R. Emmermann, Hydrothermal alteration of a 1 km section through the upper oceanic crust, DSDP Hole 504B: The mineralogy, chemistry, and evolution of seawater-basalt interactions, *J. Geophys. Res.*, *91*, 10309-10335, 1986a.

Alt, J. C., K. Muehlenbachs, and J. Honnorez, An oxygen isotopic profile through the upper kilometer of the oceanic crust, DSDP Hole 504B, *Earth Planet. Sci. Lett.*, *80*, 217-229, 1986b.

Anderko, A., and K. S. Pitzer, Equation-of-state representation of phase equilibria and volumetric properties of the system NaCl-H_2O above 573 K, *Geochim. Cosmochim. Acta*, *57*, 1657-1680, 1993.

Anderson, R. N., M. D. Zoback, S. H. Hickman, and R. L. Newmark, Permeability versus depth in the upper oceanic crust: In situ measurements in DSDP hole 504B, eastern equatorial Pacific, *J. Geophys. Res.*, *90*, 3659-3669, 1985.

Baker, E. T., A 6-year time series of hydrothermal plumes over the Cleft segment of the Juan de Fuca Ridge, *J. Geophys. Res.*, *99*, 4889-4904, 1994.

Batiza, R., Magmatic segmentation of mid-ocean ridge: A review, in *Tectonic, Magmatic, Hydrothermal and Biological Segmentation of Mid-Ocean Ridges*, edited by C. J. MacLeod, P. A. Tyler, and C. L. Walker, *Geol. Soc. Spec. Publ.*, London, *118*, 103-130, 1996.

Berndt, M. E., W. E. Seyfried Jr., and D. R. Janecky, Plagioclase and epidote buffering of cation ratios in mid-ocean ridge hydrothermal fluids: Experimental results in and near the supercritical region, *Geochim. Cosmochim. Acta*, *53*, 2283-2300, 1989.

Bischoff, J. L., and R. J. Rosenbauer, An empirical equation of state for hydrothermal seawater (3.2 percent NaCl), *Am. J. Sci.*, *285*, 725-763, 1985.

Bischoff, J. L., and R. J. Rosenbauer, Salinity variations in submarine hydrothermal systems by layered double-diffusive convection, *J. Geol.*, *97*, 613-623, 1989.

Brikowski, T., and D. Norton, Influence of magma chamber geometry on hydrothermal activity at mid-ocean ridges, *Earth Planet. Sci. Lett.*, *93*, 241-255, 1989.

Butterfield, D. A., and G. J. Massoth, Geochemistry of north Cleft vent fluids: Temporal changes in chlorinity and their possible relation to recent volcanism, *J. Geophys. Res.*, *99*, 4951-4968, 1994.

Butterfield, D. A., R. E. McDuff, M. J. Mottl, M. D. Lilley, J. E. Lupton, and G. J. Massoth, Gradients in the composition of hydrothermal fluids from the Endeavour segment vent field: Phase separation and brine loss, *J. Geophys. Res.*, *99*, 9561-9583, 1994.

Butterfield, D. A., I. R. Jonasson, G. J. Massoth, R. A. Feely, K. K. Roe, R. E. Embley, J. F. Holden, R. E. McDuff, M. D. Lilley, and J. R. Delaney, Seafloor eruptions and evolution of hydrothermal fluid chemistry, *Philos. Trans. R. Soc. London, Ser. A*, *355*, 369-386, 1997.

Cann, J. R., and M. R. Strens, Modeling periodic megaplume emission by black smoker systems, *J. Geophys. Res.*, *94*, 12,227-12,237, 1989.

Cherkaoui, A. S. M., W. S. D. Wilcock, and E. T. Baker, Thermal fluxes associated with the 1993 diking event on the coaxial segment, Juan de Fuca Ridge: A model for the convective cooling of a dike., *J. Geophys. Res.*, *102*, 24,887-24,902, 1997.

Christeson, G. L., G. M. Purdy, and G. J. Fryer, Seismic constraints on shallow crustal emplacement processes at the fast spreading East Pacific Rise, *J. Geophys. Res.*, *99*, 17,957-17,973, 1994.

Cowan, J., and J. Cann, Supercritical two-phase separation of hydrothermal fluids in the Troodos ophiolite, *Nature*, *333*, 259-261, 1988.

Delaney, J. R., R. E. McDuff, and J. E. Lupton, Hydrothermal fluid temperatures of 400°C on the Endeavour segment, northern Juan de Fuca (abstract), *Eos Trans. AGU*, *65* (45), 973, 1984.

Delaney, J. R., D. W. Mogk, and M. J. Mottl, Quartz-cemented breccias from the Mid-Atlantic Ridge: Samples of a high-salinity hydrothermal upflow zone, *J. Geophys. Res.*, *92*, 9175-9192, 1987.

Delaney, J. R., V. Robigou, R. E. McDuff, and M. K. Tivey, Geology of a vigorous hydrothermal system on the Endeavour segment, Juan de Fuca Ridge, *J. Geophys. Res.*, *97*, 19,663-19,682, 1992.

Detrick, R. S., P. Buhl, E. Vera, J. Mutter, J. Orcutt, J. Madsen, and T. Brocher, Multi-channel seismic imaging of a crustal magma chamber along the East Pacific Rise, *Nature*, *326*, 35-41, 1987.

Detrick, R. S., A. J. Harding, G. M. Kent, J. A. Orcutt, J. C. Mutter, and P. Buhl, Seismic structure of the southern East Pacific Rise, *Science*, *259*, 499-503, 1993.

Edmond, J. M., C. Measures, R. E. McDuff, L. H. Chan, R. Collier, and B. Grant, Ridge crest hydrothermal activity and the balances of the major and minor elements in the ocean: The Galapagos data, *Earth Planet. Sci. Lett.*, *46*, 1-16, 1979.

Fehn, U., and L. M. Cathles, Hydrothermal convection at slow-spreading mid-ocean ridges, *Tectonophysics*, *55*, 239-260, 1979.

Fehn, U., K. E. Green, R. P. Von Herzen, and L. M. Cathles, Numerical models for the hydrothermal field at the Galapagos spreading center, *J. Geophys. Res.*, *88*, 1033-1048, 1983.

Fornari, D. J., and R. W. Embley, Tectonic and volcanic controls on hydrothermal processes at the mid-ocean ridge: An overview based on near-bottom and submersible studies, in *Seafloor Hydrothermal Systems: Physical, Chemical, Biological, and Geological Interactions, Geophys. Monogr. Ser.*, vol. 91, edited by S. E. Humphris et al., pp. 1-46, AGU, Washington, D. C., 1995.

Forster, C., and L. Smith, Groundwater flow systems in mountainous terrain, 1, Numerical modeling techniques, *Water. Resour. Res.*, *24*, 999-1010, 1988.

Fournier, R. O., The transition from hydrostatic to greater than hydrostatic pressure in presently active continental hydrothermal systems in crystalline rock, *Geophys. Res. Lett.*, *18*, 955-958, 1991.

German, C. R., L. M. Parson, and HEAT Scientific Team, Hydrothermal exploration near the Azores triple junction: Tectonic control of venting at slow-spreading ridges?, *Earth Planet. Sci. Lett.*, *138*, 93-104, 1996.

Gillis, K. M., and P. T. Robinson, Distribution of alteration zones in the upper oceanic crust, *Geology*, *16*, 262-266, 1988.

Gillis, K. M., and P. T. Robinson, Patterns and processes of alteration in the lavas and dykes of the Troodos ophiolite, Cyprus, *J. Geophys. Res.*, *95*, 21,523-21,548, 1990.

Gillis, K. M., and G. Thompson, Metabasalts from the Mid-Atlantic Ridge: New insights into hydrothermal systems in slow-spreading crust, *Contrib. Mineral. Petrol.*, *113*, 502-523, 1993.

Gillis, K. M., G. Thompson, and D. S. Kelley, A view of the lower crustal component of hydrothermal systems at the Mid-Atlantic Ridge, *J. Geophys. Res.*, *98*, 19,597-19,619, 1993.

Goldfarb, M. S., and J. R. Delaney, Response of two-phase fluids to fracture configurations within submarine hydrothermal systems, *J. Geophys. Res.*, *93*, 4585-4594, 1988.

Gregory, R. T., and H. P. Taylor, An oxygen isotope profile in a section of Cretaceous oceanic crust, Samail ophiolite, Oman: Evidence for $D^{18}O$ buffering of oceans by deep (> 5 km) seawater-hydrothermal circulation at mid-ocean ridges, *J. Geophys. Res.*, *86*, 2727-2755, 1981.

Hayba, D. O., and S. E. Ingebritsen, Multiphase groundwater flow near cooling plutons, *J. Geophys. Res.*, *102*, 12,235-12,252, 1997.

Haymon, R. M., D. J. Fornari, M. H. Edwards, S. Carbotte, D. Wright, and K. C. Macdonald, Hydrothermal vent distribution along the East Pacific Rise crest (9°09'-54'N) and its relationship to magmatic and tectonic processes on fast-spreading mid-ocean ridges, *Earth Planet. Sci. Lett.*, *104*, 513-534, 1991.

Holmes, M. L., and H. P. Johnson, Upper crustal densities derived from bottom gravity measurements: Northern Juan de Fuca Ridge, *Geophys. Res. Lett.*, *20*, 1871-1874, 1993.

Humphris, S. E., Hydrothermal processes at mid-ocean ridges, *U. S. Natl. Rep. Int. Union Geod. Geophys. 1991-1994, Rev. Geophys.*, *33*, 71-80, 1995.

James, R. H., and H. Elderfield, Chemistry of ore-forming fluids and mineral formation in an active hydrothermal sulfide deposit on the Mid-Atlantic Ridge, *Geology*, *24*, 1147-1150, 1996.

Kelley, D. S., and J. R. Delaney, Two-phase separation and fracturing in mid-ocean ridge gabbros at temperatures greater than 700°C, *Earth Planet. Sci. Lett.*, *83*, 53-66, 1987.

Kelley, D. S., and P. T. Robinson, Development of a brine-dominated hydrothermal system at temperatures of 400-500°C in the upper level plutonic sequence, Troodos ophiolite, Cyprus, *Geochim. Cosmochim. Acta*, *54*, 653-661, 1990.

Kelley, D. S., P. T. Robinson, and J. G. Malpas, Processes of brine generation and circulation in the oceanic crust: Fluid inclusion evidence from the Troodos ophiolite, Cyprus, *J. Geophys. Res.*, *97*, 9307-9322, 1992.

Kelley, D. S., K. M. Gillis, and G. Thompson, Fluid evolution in submarine magma-hydrothermal systems at the Mid-Atlantic Ridge, *J. Geophys. Res.*, *98*, 19,579-19,596, 1993.

Kleinrock, M. C., and S. E. Humphris, Structural controls on seafloor hydrothermal activity at the TAG active mound, Mid-Atlantic Ridge, *Nature*, *382*, 149-153, 1996.

Kong, L. S. L., S. C. Solomon, and G. M. Purdy, Microearthquake characteristics of a mid-ocean ridge along-axis high, *J. Geophys. Res.*, *97*, 1659-1685, 1992.

Lister, C. R. B., On the penetration of water into hot rock, *Geophys. J. R. Astron. Soc.*, *39*, 465-509, 1974.

Lister, C. R. B., The basic physics of water penetration into hot rocks, in *Hydrothermal Processes at Seafloor Spreading Centers*, edited by P.A. Rona et al., pp. 141-168, Plenum, New York, 1983.

Little, S. A., K. D. Stolzenbach, and R. P. Von Herzen, Measurements of plume flow from a hydrothermal vent field, *J. Geophys. Res.*, *92*, 2587-2596, 1987.

Lowell, R. P., and L. N. Germanovich, On the temporal evolution of high-temperature hydrothermal systems at ocean ridge crests, *J. Geophys. Res.*, *99*, 565-575, 1994.

Lowell, R. P., and L. N. Germanovich, Evolution of a brine-saturated layer at the base of a ridge-crest hydrothermal system., *J. Geophys. Res.*, *102*, 10,245-10,255, 1997.

Lowell, R. P., P. Van Cappellen, and L. N. Germanovich, Silica precipitation in fractures and the evolution of permeability in hydrothermal upflow zones, *Science*, *260*, 192-194, 1993.

Luyendyk, B. P., On-bottom gravity profile across the East Pacific Rise crest at 21°N, *Geophysics*, *49*, 2166-2177, 1984.

Malkus, W. V. R., The heat transport and spectrum of thermal turbulence, *Proc. R. Soc. London, Ser. A*, *225*, 196-212, 1954.

Malkus, W. V. R., Statistical stability criteria for turbulent flow, *Phys. Fluids*, *8*, 1582-1587, 1996.

Malkus, W. V. R., and G. Veronis, Finite amplitude cellular convection, *J. Fluid. Mech.*, *4*, 225-260, 1958.

Manning, C. E., P. E. Weston, and K. I. Mahon, Rapid high-temperature metamorphism of East Pacific Rise gabbros from Hess Deep, *Earth Planet. Sci. Lett.*, *144*, 123-32, 1996.

McNabb, A., and J. Fenner, Thermohaline convection beneath the ocean floor, paper presented at CSIRO/DSIR Seminar on Convective Flows in Porous Media, Dep. of Sci. and Ind. Res., Wellington, New Zealand, 1985.

Meyer, C. A., R. B. McClintock, G. J. Silvestri, and R. C. Spencer Jr., *ASME Steam Tables: Thermodynamic and Transport Properties of Steam*, 436 pp., Am. Soc. of Mech. Eng., New York, 1993.

Nehlig, P., Salinity of oceanic hydrothermal fluids: A fluid inclusion study, *Earth Planet. Sci. Lett.*, *102*, 310-325, 1991.

Nehlig, P., Fracture and permeability analysis in magma-hydrothermal transition zones in the Samail ophiolite (Oman), *J. Geophys. Res.*, *99*, 589-601, 1994.

Nehlig, P., and T. Juteau, Deep crustal seawater penetration and circulation at ocean ridges: Evidence from the Oman ophiolite, *Mar. Geol.*, *84*, 209-228, 1988.

Nield, D. A., and A. Bejan, *Convection in Porous Media*, 408 pp., Springer-Verlag, New York, 1992.

Patankar, S. V., *Numerical Heat Transfer and Fluid Flow*, 153 pp., Hemisphere, Washington, D.C., 1980.

Phipps Morgan, J., and Y. J. Chen, The genesis of oceanic crust: Magma injection, hydrothermal circulation, and crustal flow, *J. Geophys. Res.*, *98*, 6283-6297, 1993.

Pitzer, K. S., J. C. Peiper, and R. H. Busey, Thermodynamic properties

of aqueous sodium chloride solutions, *J. Phys. Chem. Ref. Data, 13*, 1-106, 1984.

Ribando, T. K., K. E. Torrance, and D. L. Turcotte, Numerical models for hydrothermal circulation in the oceanic crust, *J. Geophys. Res., 81*, 3007-3012, 1976.

Richards, H. G., J. R. Cann, and J. Jensenius, Mineralogical zonation of metasomatism of alteration pipes in the Cyprus sulphide deposits, *Econ. Geol., 84*, 91-115, 1989.

Richardson, C. J., J. R. Cann, H. G. Richards, and J. G. Cowan, Metal-depleted root zones of the Troodos ore-forming hydrothermal systems, Cyprus, *Earth Planet. Sci. Lett., 84*, 243-253, 1987.

Rona, P. A., and D. A. Trivett, Discrete and diffuse heat transfer at ASHES vent field, Axial Volcano, Juan de Fuca Ridge, *Earth Planet. Sci. Lett., 109*, 57-71, 1992.

Rona, P. A., G. Klinkhammer, T. A. Nelsen, J. H. Trefry, and H. Elderfield, Black smokers, massive sulphides and vent biota at the Mid-Atlantic Ridge, *Nature, 321*, 33-37, 1986.

Rosenberg, N. D., Numerical studies of fluid flow and heat and solute transport in hydrothermal systems, Ph.D. thesis, Univ. of Calif., Santa Barbara, 1991.

Rosenberg, N. D., and F. J. Spera, Role of anisotropic and/or layered permeability in hydrothermal convection, *Geophys. Res. Lett., 17*, 235-238, 1990.

Rosenberg, N. D., F. J. Spera, and R. M. Haymon, The relationship between flow and permeability field in seafloor hydrothermal systems, *Earth Planet. Sci. Lett., 116*, 135-153, 1993.

Saccocia, P. J., and K. M. Gillis, Hydrothermal upflow zones in the oceanic crust, *Earth Planet. Sci. Lett., 136*, 1-16, 1995.

Scheirer, D. S., and K. C. Macdonald, Variation in cross-sectional area of the axial ridge along the East Pacific Rise: Evidence for the magmatic budget of a fast spreading center, *J. Geophys. Res., 98*, 7871-7885, 1993.

Schlichting, H., *Boundary Layer Theory*, 817 pp., McGraw-Hill, New York, 1979.

Schlüter, A., D. Lorenz, and F. Busse, On the stability of steady finite amplitude convection, *J. Fluid Mech., 23*, 129-144, 1965.

Schultz, A., J. R. Delaney, and R. E. McDuff, On the partitioning of heat flux between diffuse and point source seafloor venting, *J. Geophys. Res., 97*, 12,299-12,314, 1992.

Schultz, A., R. Dickson, and H. Elderfield, Temporal variations in diffuse hydrothermal flow at TAG, *Geophys. Res. Lett., 23*, 3471-3474, 1996.

Seyfried, W. E., Jr., K. Ding, and M. E. Berndt, Phase equilibria constraints on the chemistry of hot spring fluids at mid-ocean ridges, *Geochim. Cosmochim. Acta, 55*, 3559-3580, 1991.

Sinton, J. M., and R. S. Detrick, Mid-ocean ridge magma chambers, *J. Geophys. Res., 97*, 197-216, 1992.

Sleep, N. H., Hydrothermal circulation, anhydrite precipitation, and thermal structure at ridge axes, *J. Geophys. Res., 96*, 2375-2387, 1991.

Solomon, S. C., and D. R. Toomey, The structure of mid-ocean ridges, *Ann. Rev. Earth Planet. Sci., 20*, 329-364, 1992.

Sorey, M. L., Numerical modeling of liquid hydrothermal systems, *U.S. Geol. Surv. Prof. Pap., 1044-D*, 1-25, 1978.

Stakes, D. S., Oxygen and hydrogen isotope compositions of oceanic plutonic rocks: High-temperature deformation and metamorphism of oceanic layer 3, in *Stable Isotope Geochemistry: A tribute to Samuel Epstein*, edited by H. P. Taylor Jr., J. R. O'Neil, and I. R. Kaplan, *Spec. Publ. Geochem. Soc., 3*, 77-90, 1991.

Stakes, D. S., and H. P. Taylor, The northern Samail ophiolite: an oxygen isotope, microprobe and field, study, *J. Geophys. Res., 97*, 7043-7080, 1992.

Stakes, D., and D. A. Vanko, Multistage hydrothermal alteration of gabbroic rocks from the failed mathematician ridge, *Earth Planet. Sci. Lett., 79*, 75-92, 1986.

Stakes, D., C. Mevel, M. Cannat, and T. Chaput, Metamorphic stratigraphy of hole 735B, *Proc. Ocean Drill. Program Sci. Results, 118*, 153-180, 1991.

Toomey, D. R., S. C. Solomon, G. M. Purdy, and M. H. Murray, Microearthquakes beneath the median valley of the Mid-Atlantic Ridge near 23°N: Hypocenters and focal mechanisms, *J. Geophys. Res., 90*, 5443-5458, 1985.

Travis, B. J., D. R. Janecky, and N. D. Rosenberg, Three-dimensional simulation of hydrothermal circulation at mid-ocean ridges, *Geophys. Res. Lett., 18*, 1441-1444, 1991.

Tunnicliffe, V., Hydrothermal-vent communities of the deep sea, *Am. Sci., 80*, 336-349, 1992.

Von Damm, K. L., Systematics and postulated controls on submarine hydrothermal solution chemistry, *J. Geophys. Res., 93*, 4551-4561, 1988.

Von Damm, K. L., Controls on the chemistry and temporal variability of seafloor hydrothermal systems, in *Seafloor Hydrothermal Systems: Physical, Chemical, Biological, and Geological Interactions, Geophys. Monogr. Ser.*, vol. 91, edited by S. E. Humphris et al., pp. 222-247, AGU, Washington, D. C., 1995.

Von Damm, K. L., S. E. Oosting, R. Koziowski, L. G. Buttermore, D. C. Colodner, H. N. Edmonds, J. M. Edmond, and J. M. Grebmeier, Evolution of East Pacific Rise hydrothermal vent fluids following a volcanic eruption, *Nature, 375*, 47-50, 1995.

Wells, J. T., and M. S. Ghiorso, Coupled fluid flow and reaction in mid-ocean ridge hydrothermal systems: The behavior of silica, *Geochim. Cosmochim. Acta, 55*, 2467-2481, 1991.

White, D. E., Characteristics of geothermal reservoirs, in *Geothermal Energy: Resources, Production, Stimulation*, edited by P. Kruger and C. Otte, pp. 69-94, Stanford Univ. Press, Stanford, Calif, 1973.

Wilcock, W. S. D., and J. R. Delaney, Mid-ocean ridge sulfide deposits: Evidence for heat extraction from magma chambers or cracking fronts?, *Earth Planet. Sci. Lett., 149*, 49-64, 1996.

Wilcock, W. S. D., and A. McNabb, Estimates of crustal permeability on the Endeavour segment of the Juan de Fuca mid-ocean ridge, *Earth Planet. Sci. Lett., 138*, 83-91, 1995.

Wolfe, C. J., G. M. Purdy, D. R. Toomey, and S. C. Solomon, Microearthquake characteristics and crustal velocity structure at 29°N on the Mid-Atlantic Ridge: The architecture of a slow spreading segment, *J. Geophys. Res., 100*, 24,449-24,472, 1995.

Yang, J., R. N. Edwards, J. W. Molson, and E. A. Sudicky, Three-dimensional numerical simulation of the hydrothermal system within TAG-like sulfide mounds, *Geophys. Res. Lett., 23*, 3475-3478, 1996.

Yusufova, V. D., R. I. Pepinov, V. A. Nicolayev, G. U. Zokhrabbekova, N. V. Lobcova, and T. D. Tuayev, Thermophysical properties of softened seawater and salt solutions over a wide temperature and pressure range, *Desalination, 25*, 269-280, 1978.

W. S. D. Wilcock, School of Oceanography, University of Washington, Box 357940, Seattle, WA 98195-7940. (e-mail: wilcock@ocean.washington.edu)

(Received May 14, 1997; revised October 6, 1997;
accepted November 5, 1997.)